PHYSICAL REVIEW D **75,** 035006 (2007)

Direct detection of supersymmetric particles in neutrino telescopes

Ivone F. M. Albuquerque and Gustavo Burdman
Instituto de Física, Universidade de São Paulo, São Paulo, Brazil

Z. Chacko
Department of Physics, University of Arizona, Tucson, Arizona 85721, USA
(Received 22 May 2006; revised manuscript received 16 October 2006; published 12 February 2007)

In supersymmetric theories where the lightest supersymmetric particle is the gravitino the next to lightest supersymmetric particle is typically a long-lived charged slepton. In this paper, following our earlier proposal [I. Albuquerque, G. Burdman, and Z. Chacko, Phys. Rev. Lett. **92**, 221802 (2004).], we perform a detailed study of the production of pairs of these particles induced by the interactions of high energy cosmic neutrinos with nucleons in the Earth, their propagation through the Earth, and finally their detection in neutrino telescopes. We investigate the charged slepton energy loss in detail and establish that the relatively small cross section for the production of supersymmetric particles is partially compensated for by the very long range of these heavy particles. The signal, consisting of two parallel charged tracks emerging from the Earth, is characterized by a track separation of a few hundred meters. We perform a careful analysis of the main background, coming from direct di-muon production, and show that it can be separated from the signal due to its characteristically smaller track separation. We conclude that neutrino telescopes will complement collider searches in the determination of the supersymmetry breaking scale, and may even provide the first evidence for supersymmetry at the weak scale.

DOI: 10.1103/PhysRevD.75.035006 PACS numbers: 14.80.Ly, 11.30.Pb, 12.60.Jv, 95.30.Cq

I. INTRODUCTION

One of the most pressing questions in particle physics is the origin and stability of the hierarchy between the weak and the Planck energy scales. Natural solutions of this so-called hierarchy problem require new physics at the TeV scale. One of the most attractive candidate theories is weak scale supersymmetry. Although this is in no small measure due to its theoretical appeal (it is a simple and natural extension of the usual space-time symmetries), it is also favored by data from electroweak observables. These point to a weakly coupled Higgs sector, one without significant deviations from the standard model in regard to electroweak precision observables, as arises naturally in supersymmetric (SUSY) theories. However, supersymmetry must be broken since the superpartners have not yet been observed. The supersymmetric spectrum is determined by the supersymmetry breaking mechanism.

Supersymmetric theories typically possess a discrete symmetry, R-parity, which ensures that corrections to precision electroweak observables are small. The existence of this discrete symmetry immediately implies that the lightest supersymmetric particle (LSP) is stable. Which of the supersymmetric particles is the LSP is determined by the scale of supersymmetry breaking, which we denote by $\sqrt{F}$. When supersymmetry is broken at high scales such that $\sqrt{F} \gtrsim 10^{10}$ GeV the LSP is typically the neutralino. If however supersymmetry is broken at lower scales, $\sqrt{F} \lesssim 10^{10}$ GeV, the LSP tends to be the gravitino. In models where the LSP is the gravitino, the next to lightest supersymmetric particle (NLSP) is usually a charged slepton, typically the right-handed stau. When the supersymmetry breaking scale $\sqrt{F}$ is much larger than a TeV, the stau NLSP decays to gravitinos through interactions that are extremely small, and therefore its lifetime can be very large. In gauge-mediated SUSY breaking, for instance, we have

$$c\tau = \left(\frac{\sqrt{F}}{10^7\ \text{GeV}}\right)^4 \left(\frac{100\ \text{GeV}}{m_{\tilde{\tau}_R}}\right)^5 10\ \text{km}, \qquad (1.1)$$

where $m_{\tilde{\tau}_R}$ is the stau mass. Thus, for $\sqrt{F} \gtrsim 10^7$ GeV if these NLSPs were to be produced by very high energy collisions they could travel very long distances before decaying.

Many interesting and realistic supersymmetric models have been proposed where the scale of supersymmetry breaking $\sqrt{F}$ is larger than 5×10^6 GeV and where the LSP is the gravitino while the NLSP is a long-lived stau. These include models of low energy supersymmetry breaking such as gauge mediation [1], but also superWIMP scenarios [2], where the supersymmetry breaking scale is much higher and the NLSPs decay to the gravitino only on very large time scales of about a year.

In a recent letter [3], we proposed that the diffuse flux of high energy neutrinos colliding with the Earth could produce pairs of slepton NLSPs which due to their large range could travel large distances through the Earth and be detected in neutrino telescopes. The neutrino-nucleon reaction can produce a pair of supersymmetric particles that will promptly decay to a pair of NLSPs and standard model (SM) particles. This process results in NLSPs which typically have a very high boost and therefore will not decay inside the Earth provided the supersymmetry breaking

scale $\sqrt{F} > 10^7$ GeV. (For $5 \times 10^6 < \sqrt{F} < 10^7$ GeV a significant fraction of the decays will occur inside the Earth.) Since the NLSP is charged, its upward going tracks could in principle be detected in large ice or water Cerenkov detectors, such as IceCube [4]. This is in analogy with the standard model charged current interaction giving muons, the primary signal in neutrino telescopes. The high boost and large range of the NLSPs implies that the tracks are parallel and well separated, enabling them to be distinguished from background events. Various aspects of this scenario were further considered in Refs. [5–7].

In principle, one could think that cosmic rays could be an even better source of supersymmetric events, and ultimately of NLSPs. After all, if one considers a proton primary, squark pair production should be larger than the slepton production via neutrino interactions, due to the fact that it goes through a larger coupling. However, this cannot compete with the soft, forward cross section of cosmic rays with air, which is large enough to stop primaries in the atmosphere. Typical cross sections for cosmic ray primaries in the Earth's atmosphere are around 10–100 mb, so that the atmosphere is several interaction lengths. On the other hand, supersymmetric production cross sections at the energies of interest are in the order of 10–100 pb, or 10^{-9} times smaller. Thus, the probability of producing supersymmetric events with proton or other cosmic ray primaries is very small. Neutrinos, on the other hand, will always go through the atmosphere, with enough of them interacting inside the Earth within the range of the NLSP from the detector. Then, since the neutrino flux is not expected to be that much smaller than the cosmic ray flux, using neutrinos is advantageous.

In this paper we present a detailed analysis of the original proposal [3]. We perform a careful study of the production of supersymmetric particles, their propagation through the Earth, and their detection in neutrino telescopes. We compute the expected number of signal events in IceCube, their characteristic energy distribution, and the energy deposited in the detector. We also investigate the main background, which arises from di-muon production, and verify that it can be separated from the signal by making suitable cuts.

In analyzing the signal, it is particularly important to carefully incorporate the energy losses involved in the propagation of sleptons through the Earth. Although bremsstrahlung and pair-production energy loss become less important for heavy charged particles, photonuclear energy loss potentially presents a problem. In fact, at first this appears to be a great obstacle since it is known that photonuclear energy loss dominates the propagation of tau leptons [8,9]. However, this is not the case. As we already sketch in Ref. [3] and was shown by the explicit calculation in Ref. [6], there is a mass suppression of the photonuclear energy loss, which manifests itself for masses well above that of the τ and affects the energy loss of a particle such as the $\tilde{\ell}_R$. We will reproduce the results of Ref. [6] regarding the photonuclear energy loss of a slepton, and explicitly show how the mass suppression comes about and why it is not operative for the τ energy loss. As a result, the photonuclear energy losses for heavy charged particles, whether scalars such as the NLSP or fermions such as heavy leptons, are suppressed due to their large masses.

The main background to the signal arises from di-muon events which also give rise to pairs of tracks in the detector. However, we show that these can be readily distinguished from the signal by the separation between tracks. The key point is that the NLSP range is much larger than the muon range, which is only of the order of a few kilometers. Therefore, while the typical track separation in the detector for the NLSP signal is of order a few hundred meters, direct di-muon production results in tracks that are typically closer together by an order of magnitude.

The plan for the paper is as follows: we review in detail the relevant cross section for supersymmetric production in Sec. II. In Sec. III we study in detail the energy loss of sleptons as they travel through the Earth. An analysis of the signal and backgrounds is presented in Sec. IV and we conclude with a discussion of our results in Sec. V.

II. CROSS SECTIONS

In this section we summarize the calculation of the production cross section for the NLSP pair. The supersymmetric process of interest involves the t-channel production of a slepton and a squark via gaugino exchange. For simplicity, we neglect mixing with Higgsinos in the gaugino sector. Then the processes analogous to the charged current (CC) in the SM is $\nu N \to \tilde{\ell}_L \tilde{q}$, where $\tilde{q}$ can be an up- or down-type squark, and the particle exchanged in the t-channel is a chargino. These are shown in Figs. 1(a) and 1(b), and are the dominant contributions. The neutrino, always produced left-handed by the weak interactions, can interact either with a left-handed down-type quark (a), or with a right-handed up-type antiquark (b). This results in the partonic cross sections:

$$\frac{d\sigma^{(a)}}{dt} = \frac{\pi\alpha}{2\sin^4\theta_W} \frac{M_{\tilde{w}}^2}{s(t - M_{\tilde{w}}^2)^2} \tag{2.1}$$

$$\frac{d\sigma^{(b)}}{dt} = \frac{\pi\alpha}{2\sin^4\theta_W} \frac{(tu - m_{\tilde{\ell}_L}^2 m_{\tilde{q}}^2)}{s^2(t - M_{\tilde{w}}^2)^2}, \tag{2.2}$$

where s, t, and u are the usual Mandelstam variables, and $M_{\tilde{w}}$, $m_{\tilde{\ell}_L}$, and $m_{\tilde{q}}$ are the chargino, the left-handed slepton, and the squark masses, respectively. The left-handed slepton and the squark decay promptly to the lighter "right-handed" slepton plus nonsupersymmetric particles. We also include the subdominant neutralino exchange, Figs. 1(c) and 1(d).

We take $m_{\tilde{w}} = 250$ GeV, $m_{\tilde{\ell}_L} = 250$ GeV, and three values for the squark masses: $m_{\tilde{q}} = 300$, 600, and

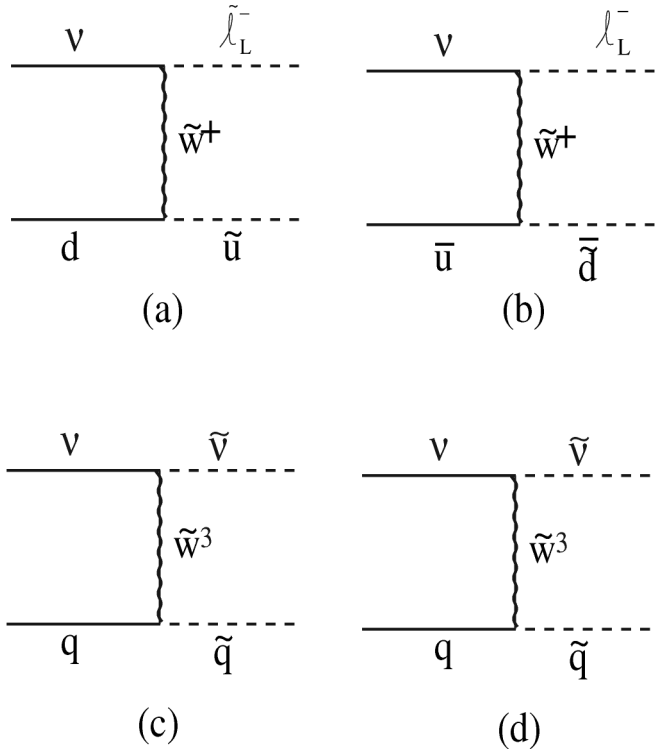

FIG. 1. Feynman diagrams for supersymmetric particle production in νN collisions charged current (chargino) interactions: (a) Left-left interaction requiring the insertion of the gaugino mass in the t-channel line. (b) Left-right interaction. Neutral current: (c), (d). There are analogous diagrams for antineutrinos as well as for strange and charm initial quarks.

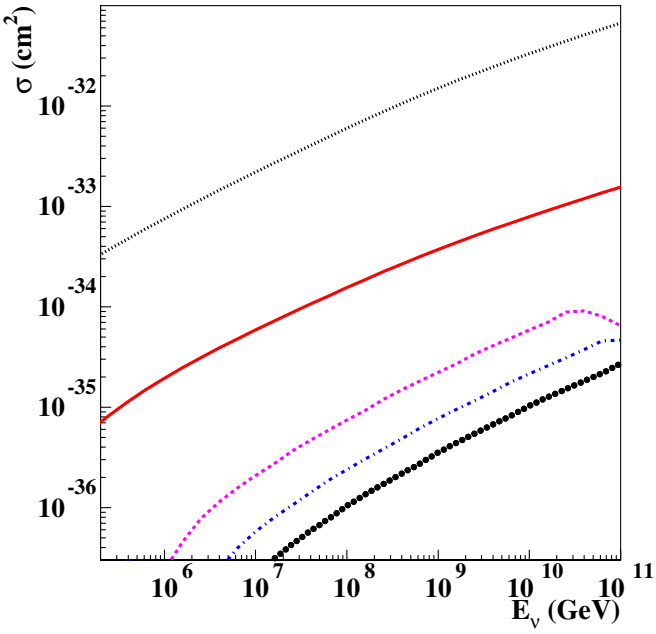

FIG. 2 (color online). νN cross sections vs the energy of the incident neutrino. The three lower curves correspond to $m_{\tilde{\ell}_L} = 250$ GeV, $m_{\tilde{w}} = 250$ GeV; and for squark masses $m_{\tilde{q}} = 300$ GeV (dashed), 600 GeV (dot-dashed) and 900 GeV (dotted). The top curve corresponds to the SM charged current interactions and the middle one to the di-muon background.

900 GeV. These are very representative values in the scenarios under consideration. This is clearly the case for gauge-mediated supersymmetry breaking, where superpartner masses are generated by their interactions. Then, typically the $\tilde{\tau}_R$ is the NLSP, being heavier only than the ultralight and very weakly coupled gravitino. Charginos and neutralinos tend to be heavier since they also feel the $SU(2)_L$ interactions. Finally, squarks are heavier still since their masses are affected by the strong interactions. In Fig. 2 we plot the cross sections for supersymmetric production in νN interactions as a function of the neutrino energy. Also plotted for comparison is the SM charged current (top curve) and the di-muon (second from top) cross sections.

Every supersymmetric event produces a $\tilde{\ell}_L$ and $\tilde{q}$ as primaries, which then decay. The resulting cascades always leave a pair of $\tilde{\ell}_R$ and SM particles. In what follows we will take $m_{\tilde{\ell}_R} = 150$ GeV. The SUSY cross sections are considerably suppressed with respect to the SM, even when well above threshold. This is to be expected since the SM cross section is dominated by very small values of x, whereas for the SUSY processes one always needs to be above a rather large threshold, resulting in $x > m^2_{\rm SUSY}/(2M_P E_\nu)$, where $m_{\rm SUSY}$ is the typical mass of the supersymmetric particles being produced. However, we will see that this will be compensated by the very long range of sleptons compared with the muon range, which is only a few kilometers.

III. NLSP ENERGY LOSS

Once produced by the νN interactions in the Earth, the pair of NLSPs should range into the detector, just as the muons produced by CC events [10]. Charged particles lose energy due to ionization processes as well as through radiation. The average energy loss can be written as [11]

$$-\frac{dE}{dx} = a(E) + b(E)E, \tag{3.1}$$

where $a(E)$ characterizes the ionization losses, and $b(E)$ includes the contributions to radiation energy losses from various sources including bremsstrahlung, pair production, and photonuclear interactions.

A. Ionization

Ionization energy loss can be approximated by the Bethe-Block formula [11]

$$\left(-\frac{dE}{dx}\right)_i = 2\pi N_A r_e^2 m_e c^2 \frac{z^2}{\beta^2}\frac{Z_a}{A_a}\left\{\ln\left(\frac{4m_e^2 c^2 v^2 \gamma^2 (\beta\gamma)^2}{I^2}\right) - 2\beta^2 - \delta - \frac{C}{Z_a}\right\}. \tag{3.2}$$

In Eq. (3.2), N_A is Avogadro's number, r_e is the classical electron radius, m_e its mass, Z_a and A_a the atomic number and mass of the absorber, respectively, and z the charge of the incident particle in units of e, the electron charge. The mean ionization potential I is typically of about 100 eV (136 eV for standard rock). The density correction δ reflects the effect of the polarization of the medium as the incident particle's energy increases. This reduces the energy loss at high energies. For the case of the NLSP in question, this reduction is still small and of the order of 10%. Finally, the shell correction C taking into account the effects of atomic bounding, are only important for small values of $\beta\gamma$, similar to the bound electrons'. For $\beta\gamma \simeq 0.3$ this correction is about 1%. For the much larger values of $\beta\gamma$ relevant here, this correction is negligible. Therefore, the ionization loss can be parametrized by

$$a(\beta\gamma) \simeq 0.08 \frac{\text{MeV cm}^2}{\text{gr}} (17 + 2\ln\beta\gamma), \tag{3.3}$$

and is rather independent of the particle mass. For instance, for a density of $\rho = 2.5$ gr/cm^3, roughly corresponding to standard rock in the Earth's crust, and for $\beta\gamma = 10^5$, we have $a \simeq 8$ MeV/cm. However, at these values of $\beta\gamma$ most of the energy loss will occur through radiation.

B. Radiation energy loss

At sufficiently large energies the energy loss due to radiation processes dominates over ionization for all charged particles. For instance, for muons this dominance takes place at energies of several hundred GeV. The radiation loss can be written as

$$b(E) = \frac{N_A}{A} \int_{y_{\min}}^{y_{\max}} y \frac{d\sigma}{dy} dy, \tag{3.4}$$

where N_A is Avogadro's number, A is the atomic mass of the target, and y is the fractional energy loss of the (s)lepton

$$y \equiv \frac{E - E'}{E}, \tag{3.5}$$

with E' the final lepton energy in the target's rest frame. Although there is no simple scaling with mass, heavier particles such as NLSPs will have suppressed radiative energy losses. In what follows we discuss the differential cross section $d\sigma/dy$ for radiative energy loss of NLSPs due to bremsstrahlung, pair production, and photonuclear interactions.

1. Bremsstrahlung

The differential cross section for bremsstrahlung is reviewed in detail in Ref. [12]. The contribution from the interaction with the screened nucleus dominates and is given by

$$\left(\frac{d\sigma}{dy}\right)_{\text{brem,nucl}} = \alpha\left(2Z\frac{m_e}{m_\ell} r_e\right)^2 \left(\frac{4}{3} - \frac{4}{3}y + y^2\right) \frac{\Phi(\delta)}{y}, \tag{3.6}$$

where m_ℓ is the mass of the interacting (s)lepton,

$$\Phi(\delta) = \ln\left(\frac{Bm_\ell Z^{-1/3}/m_e}{1 + \delta\sqrt{e}BZ^{-1/3}/m_e}\right) - \ln\left(\frac{D_n}{1 + \delta(D_n\sqrt{e} - 2)/m_\ell}\right), \tag{3.7}$$

and we have defined

$$\delta = \frac{m_\ell y}{2E(1 - y)},$$

and

$$D_n = 1.54A^{0.27}. \tag{3.8}$$

Finally, r_e is the classical electron radius and in this case $B = 182.7$. There is also a subdominant contribution from the bremsstrahlung induced by atomic electrons. This is down by a factor of Z with respect to Eq. (3.6). It is possible to approximate this effect by replacing Z^2 in Eq. (3.6) by $Z(Z + 1)$. In order to obtain $b_{\text{brem}}(E)$ we must integrate y, with $y_{\min} = 0$ and $y_{\max} = 1 - (3/4)\sqrt{e}Z^{1/3}(m_\ell/E)$.

As it can be seen by comparing Fig. 3 and Fig. 5, the bremsstrahlung contributions are greatly suppressed for the slepton case compared to the muon. This can already be seen in the expression (3.6), by the appearance of a factor $1/m_\ell^2$. Thus, for the NLSP case, with masses in the hundreds of GeV, this contribution will be negligible.

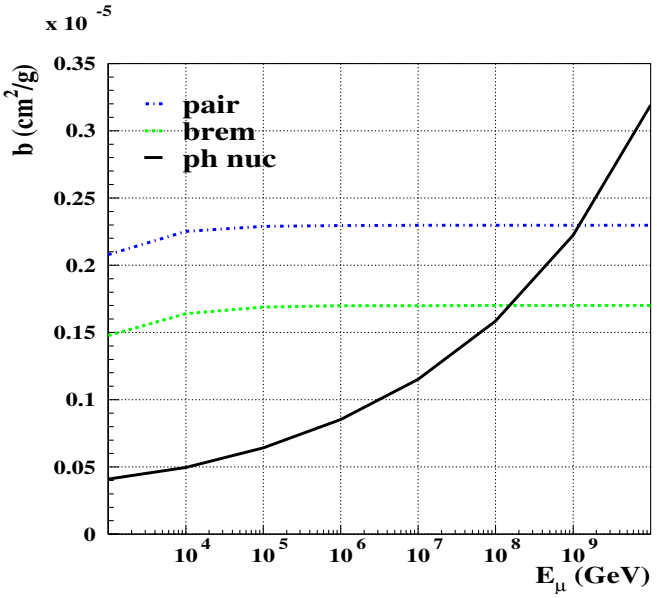

FIG. 3 (color online). The muon energy loss function $b(E)$ defined by Eqs. (3.1) and (3.4).

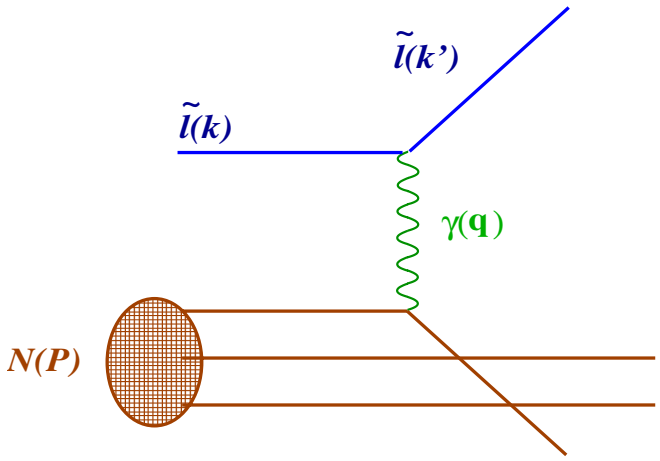

FIG. 4 (color online). The scattering $\tilde{\ell}(k)N(P) \rightarrow \tilde{\ell}(k')X$ in the deep inelastic picture.

2. Pair production

As was noted in Ref. [6], the dominant contributions to energy loss due to pair production come from diagrams which are independent of the spin of the heavy lepton. Then it is possible to accurately estimate this contribution to $b(E)$ by considering a heavy lepton, instead of a scalar lepton as it would be the case for the NLSP. The fermion and scalar cases are almost identical at the high energies considered here. A compete QED calculation of the direct pair production was done in Ref. [13]. Based on this, a useful parametrization for the double differential cross section is given in Ref. [14]:

$$\frac{d^2\sigma}{dyd\rho} = \alpha^4(Z\lambda_e)^2\frac{1-y}{y}\left(\phi_e + \frac{m_e^2}{m_{\tilde{\ell}}^2}\phi_\mu\right), \tag{3.9}$$

where λ_e is the electron's Compton wavelength and $\rho \equiv (E^+ - E^-)/(E^+ + E^-)$ is the asymmetry parameter of the pair. The functions ϕ_e and ϕ_μ correspond to different QED diagrams and include corrections for atomic and nuclear form-factors. Their form can be found, for instance, in Ref. [12]. Just as in the bremsstrahlung case, and in order to take into account the contribution from atomic electrons, we can simply replace Z^2 in Eq. (3.9) by $Z(Z+1)$. Then, the energy loss due to pair production is computed as

$$b_{\text{pair}}(E) = \frac{N_A}{A}\int_{y_{\min}}^{y_{\max}}\int_0^{\rho_{\max}} y\frac{d^2\sigma}{dyd\rho}dyd\rho. \tag{3.10}$$

Here, the integration limits are

$$\frac{4m_e}{E} \le y \le 1 - \frac{3}{4}\sqrt{e}Z^{1/3}\frac{m_\ell}{E} \quad \text{and}$$
$$0 \le \rho \le \left(1 - \frac{6m_\ell^2}{(1-y)E^2}\right)\sqrt{1 - \frac{4m_e}{yE}}. \tag{3.11}$$

The energy loss by $e^+ - e^-$ pair production for a muon is plotted in Fig. 3 and that for a slepton with $m_{\tilde{\ell}} = 150$ GeV in Fig. 5 (dot-dashed curves). Once again, it is clear that the energy loss is suppressed in the case of the heavier (s)lepton. Although pair creation is an important source of energy loss in the slepton propagation, it is not the most important one, as we will see next.

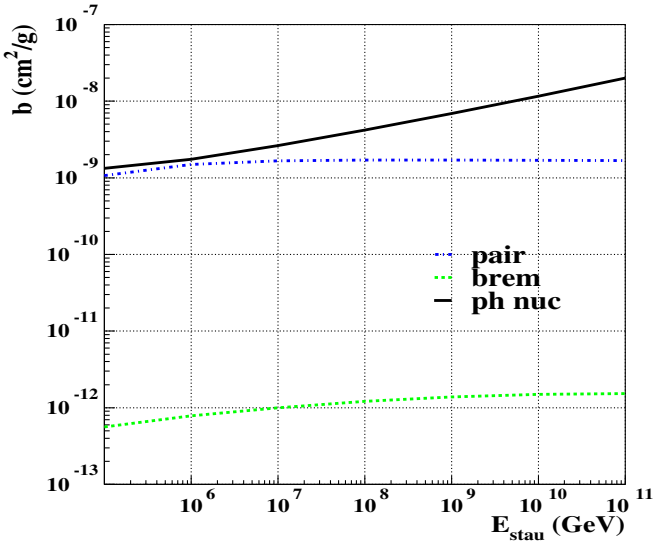

FIG. 5 (color online). The slepton energy loss function $b(E)$ defined by Eqs. (3.1) and (3.4).

3. Photonuclear energy loss

For a heavy particle such as the slepton NLSP, the most important source of energy loss is the photonuclear interactions. These already dominate the τ energy loss. However, as we will see below, there will still be a considerable suppression due to the NLSP mass. This mass dependence is subtle, so we spend some time discussing its origin. We compute the scattering of a scalar such as the $\tilde{\ell}$ NLSP off a nucleon (see Fig. 4) following the deep inelastic formalism. In general the cross section can be expressed as

$$d\sigma = \alpha^2\frac{1}{EE'Q^4}L_{\mu\nu}W^{\mu\nu}d^3k', \tag{3.12}$$

where $E(E')$ is the incoming (outgoing) electron energy, $\vec{k}'$ is the outgoing slepton momentum, and $Q^2 = -q^2 = (k - k')^2$ is the photon virtuality, k and k' are the four-momenta of the incoming and outgoing slepton, respectively. The momentum fraction of the struck quark is described by the Bjorken variable

$$x = \frac{Q^2}{2P\cdot q} = \frac{Q^2}{2M(E-E')}, \tag{3.13}$$

with P and M the four-momentum and mass of the nucleon, respectively. The hadronic tensor is parametrized as usual in terms of two structure functions, $F_1(x, Q^2)$ and $F_2(x, Q^2)$:

$$W_{\mu\nu} = -\frac{F_1}{M} g_{\mu\nu} + \frac{F_2}{M^2 Ey} P_\mu P_\nu + \left(\frac{F_1}{M} + F_2 \frac{Ey}{q^2}\right)\frac{q_\mu q_\nu}{q^2} - \frac{F_2}{M}\frac{P_\mu q_\nu + P_\nu q_\mu}{q^2}. \quad (3.14)$$

In the Callan-Gross limit, the hadronic form factors are related by

$$2xF_1(x, Q^2) = \left(1 + \frac{4M^2x^2}{Q^2}\right)F_2(x, Q^2). \quad (3.15)$$

More generally, departure from this limit can be parametrized by the function $R(x, Q^2)$ defined by

$$R(x, Q^2) = \frac{F_L(x, Q^2)}{2xF_1(x, Q^2)}, \quad (3.16)$$

where the longitudinal structure function is

$$F_L(x, Q^2) = \left(1 + \frac{4M^2x^2}{Q^2}\right)F_2(x, Q^2) - 2xF_1(x, Q^2). \quad (3.17)$$

Thus, we can eliminate $F_1(x, Q^2)$ in favor of $F_2(x, Q^2)$ and $R(x, Q^2)$, where the latter function vanishes in the deep inelastic limit.

On the other hand, the slepton tensor is given by

$$L_{\mu\nu} = (k + k')_\mu (k + k')_\nu. \quad (3.18)$$

We can now compute the double differential cross section in terms of the structure function $F_2(x, Q^2)$ as well as the Callan-Gross violating function $R(x, Q^2)$. The result is given by

$$\frac{d^2\sigma}{dydQ^2} = \frac{\pi\alpha^2}{Q^4}\frac{F_2(x, Q^2)}{y}\left\{(2 - y)^2 - y^2\left(1 + \frac{4m_{\tilde{\ell}}^2}{Q^2}\right) \times \frac{(1 + \frac{4M^2x^2}{Q^2})}{(1 + R(x, Q^2))}\right\}, \quad (3.19)$$

which agrees with Ref. [6]. In order to obtain the photonuclear energy loss function we have

$$b_{\text{ph-nuc}}(E) = \frac{N_A}{A}\int_{y_{\min}}^{y_{\max}} dy \int_{Q^2_{\min}}^{Q^2_{\max}} y\frac{d\sigma}{dydQ^2}, \quad (3.20)$$

where $y_{\min} = ((M + m_\pi)^2 - M^2)/2ME$, $y_{\max} = 1 - m_{\tilde{\ell}}/E$, $Q^2_{\max} = 2MEy - ((M + m_\pi)^2 - M^2)$, and the minimum photon virtuality is given by

$$Q^2_{\min} = 2[E^2(1 - y) - kk' - m_{\tilde{\ell}}^2] \simeq \frac{m_{\tilde{\ell}}^2 y^2}{(1 - y)}, \quad (3.21)$$

and corresponds to a forward slepton. The last expression in Eq. (3.21) reflects the approximation for small values of the slepton energy loss ($y \ll 1$). The Callan-Gross limit is an excellent approximation in the energies of interest here, so we will take $R(x, Q^2) = 0$ from now on. We must now specify the structure function $F_2(x, Q^2)$. We use the ALLM parametrization [15,16], which fits nicely all data from very low Q^2 to $Q^2 = 5000$ GeV^2. The parametrization has a $\chi^2/\text{ndf} = 0.97$ for a total of 1356 points. The details of the parametrization used here can be found in the update of Ref. [16].

In addition, we must account for nuclear shadowing, which can be an important effect at low values of x. This is done by defining the ratio

$$a(A, x, Q^2) = \frac{F_2^A(x, Q^2)}{AF_2^N(x, Q^2)}, \quad (3.22)$$

where $F_2^A(x, Q^2)/A$ and $F_2^N(x, Q^2$ are the nuclear and the free nucleon structure functions, respectively. A parametrization of this ratio describing the data is given in Ref. [8]. It is found to be rather Q^2-independent and is given by

$$a(A, x) = \begin{cases} A^{-0.1} & x < 0.0014 \\ A^{0.069\log_{10}+0.097} & 0.0014 \le x \le 0.04 \\ 1 & 0.04 < x. \end{cases}$$

Assuming that $Z = A/2$, the structure function F_2^A can be obtained as

$$F_2^A = a(A, x)\frac{A}{2}(1 + P(x))F_2^p. \quad (3.23)$$

In Eq. (3.23) F_2^p is the proton structure function and $P(x) = 1 - 1.85x + 2.45x^2 - 2.35x^3 + x^4$ describes the F_2^n/F_2^p ratio as a fit to the Bologna-Cern-Dubna-Munich-Saclay Collaboration data.

The photonuclear energy loss can now be computed using Eq. (3.20) with the structure function $F_2^p(x, Q^2)$ that is extracted from data and parametrized by ALLM. We plot the result in Fig. 5 (solid curve).

We observe that the photonuclear energy loss appears to be also suppressed for higher masses when compared with the muon case, as can be seen from Fig. 3 (solid curve). This seems odd at first, since the effect is larger for the τ than it is for the μ [8,9]. In order to understand this mass dependence for the heavier masses, we should note that the cross section that determines the structure function $F_2^p(x, Q^2)$ is dominated by physics at rather low Q^2 ($\simeq 1$ GeV^2), where resonances and other nonperturbative effects set in. However, we see from Eq. (3.21) that for large slepton masses the minimum value of the photon virtuality is typically larger than this, unless the energy loss y is very small. Thus, the most important contributions to the structure function are left out as a consequence, leading to a suppression for sufficiently large masses $m_{\tilde{\ell}}^2 \gg 1$ GeV^2. This explains why the effect is still large for the τ but then is suppressed for heavier (s)leptons.

Finally, we consider the possible electroweak contributions to the slepton energy loss, where the photon is replaced by either a gauge boson or a gaugino. Since the propagating slepton is ''right-handed,'' it only has neutral interactions. Of these, the dominant contribution comes

from the exchange of a Z boson. For this to begin to be comparable to the photonuclear process described above, we need $Q^2 \gtrsim M_Z^2$. However, as mentioned earlier, the structure functions are dominated by the low Q^2 region. Thus, we expect the Z-exchange contribution to be suppressed by this effect. The results of the explicit calculation confirm this expectation. The energy loss due to Z-exchange is at least 2 orders of magnitude smaller than the photonuclear energy loss, and even smaller for most of the energies of interest. As a source of energy loss it is also smaller than the pair production, and is only larger than bremsstrahlung for slepton energies above 10^7 GeV.

In what follows we will make use of the calculations of the energy loss for an NLSP in order to compute the number of events ranging into the IceCube detector.

IV. SIGNALS IN NEUTRINO TELESCOPES

A. Neutrino flux

In order to compute the event rates in neutrino telescopes, we need to know the incoming neutrino flux. The presence of cosmic neutrinos is expected on the basis of the existence of high energy cosmic rays. Several estimates of the neutrino flux are available in the literature. In most cases, it is expected that km^3 neutrino telescopes will measure this flux. Here we will make use of two calculations of the neutrino flux in order to compute the number of expected NLSP events at neutrino telescopes.

First, we consider the work of Waxman and Bahcall (WB) [17], who pointed out that the observed cosmic ray flux implies an upper bound on the high energy astrophysical neutrino flux. This argument requires that the sources be optically "thin," meaning that most of the protons escape and only a fraction of them interact inside the source. In order to determine the neutrino spectrum, WB fix the cosmic ray spectral index to -2, giving

$$\left(\frac{d\phi_\nu}{dE}\right)_{\rm WB} = \frac{(1-4)\times 10^{-8}}{E^2}\ {\rm GeV\,cm^{-2}\,s^{-1}\,sr^{-1}}, \quad (4.1)$$

where the range in the coefficient depends on the cosmological evolution of the sources. Using the upper end we obtain the so-called WB limit.

On the other hand, Manheim, Proterhoe, and Rachen (MPR) [18] obtain an upper limit on the diffuse neutrino sources in a way that is somewhat different than WB. Instead of assuming a fixed cosmic ray index for the spectrum, MPR determine the spectrum directly from data at each energy. In the case when the sources are considered optically thin, this procedure results in a limit similar to that of WB for energies between 10^7 and 10^9 GeV and larger otherwise.

We consider an initial flux containing both ν_μ and ν_e (in a 2:1 ratio). Since the initial interactions (see Fig. 1) produce $\tilde{\ell}_L$ and these are nearly degenerate in flavor, the flavor of the initial neutrino does not affect our results. For the same reason, the possibility of large mixing in the neutrino flux is also innocuous here.

B. NLSP Signals

Having the neutrino flux from the previous section, the production cross section for NLSP pairs (Sec. II), and their energy loss (Sec. III) through Earth, we can now compute the number of NLSP events at neutrino telescopes. In order to correctly take into account the propagation of neutrinos and the NLSP $\tilde{\ell}_R$ through the Earth, we make use of a model of the Earth density profile as detailed in Ref. [19].

In Fig. 6 we show the energy distribution for the NLSP pair events for three choices of squark masses: 300 GeV, 600 GeV, and 900 GeV. Also shown are the neutrino flux at Earth in the WB limit, as well as the energy distribution of upgoing μ's, and that of direct $\mu^+\mu^-$ production (see Sec. IV C). We see that, even for the heavier squarks, it is possible to obtain observable event rates. In Table I we show the event rates for $\tilde{\ell}_R$ pair production per year and per km^2. The rates are given for the WB flux as well as for the MPR flux [18], both for optically thin sources. For comparison, we also show the rates for the $\mu^+\mu^-$ background. Thus, km^3 Cerenkov detectors such as IceCube appear to be sensitive to most of the parameter space of interest in

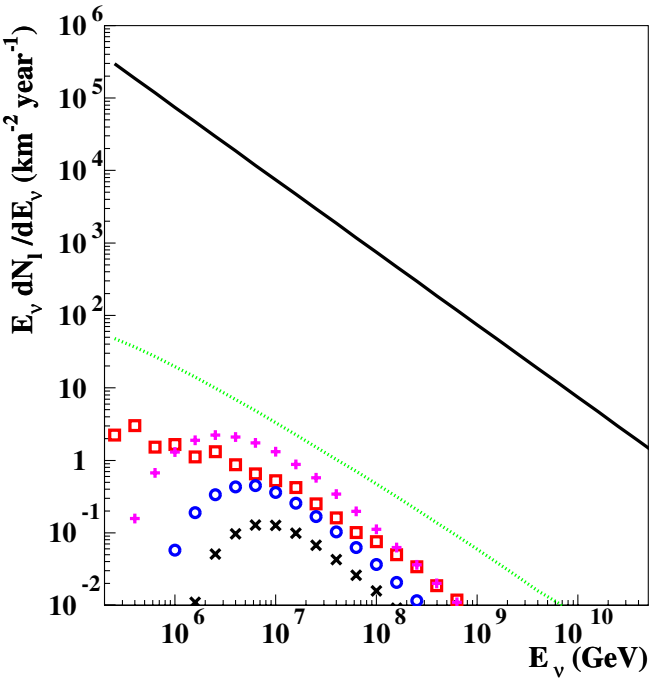

FIG. 6 (color online). Energy distribution of $\tilde{\ell}_R$ pair events per km^2, per year, at the detector. Curves that do not reach the y axis; from top to bottom: $m_{\tilde{q}} = 300$, 600, and 900 GeV. Here, $m_{\tilde{\ell}_R} = 150$ GeV and $m_{\tilde{w}} = 250$ GeV. Also shown are the neutrino flux at Earth and the μ and the di-muon flux through the detector (curves that reach the y axis; from top to bottom, respectively). In all cases we make use of the WB limit for the neutrino flux.

TABLE I. Number of events per km^2 per year for different neutrino fluxes at the Earth. The $\tilde{\ell}_R$ mass is 150 GeV and squark masses are 300, 600, and 900 GeV, respectively. The signal events are integrated from threshold ($E_\nu > 1.6 \times 10^5$ GeV), whereas the number of di-muon events are given for neutrino energies above 10^3 GeV. The column $\mu^+\mu^-$ corresponds to the di-muon background before track separation cuts are applied (see Sec. IV C).

		$\tilde{\ell}_R\tilde{\ell}_R$		
	$\mu^+\mu^-$	(300)	(600)	(900)
WB	30	6	1	0.3
MPR	1412	21	3	1

scenarios with a relatively long-lived NLSP. The rates are comparable to the ones we obtained in Ref. [3].

The NLSPs are produced in pairs very far from the detector and with a very large boost. Although the angle between the two NLSP tracks is small due to the boost, the large range means that there will be a significant separation between the tracks. The question is then whether this separation is large enough to be observed, but not too large so as to be larger than the dimensions of the detector. A rough estimate can be made by defining the separation between NLSP tracks as $\delta R \simeq L\theta$, with L the distance to the production point, typically a few 1000 Km and $\theta \simeq p^{\rm CM}_{\rm SUSY}/p_{\rm boost} \simeq (10^{-4}$–$10^{-5})$, the typical angle between the NLSPs in the lab frame. Then we should expect that the typical separation between the two NLSP tracks is of the order of $\delta R \simeq$ few $\times$ (10–100) m.

We performed a more detailed calculation in order to have a more precise prediction for the distribution of the track separation of the events. We consider the angular distribution of the two primaries in the center of mass, as implied by Eqs. (2.1) and (2.2) as well as those of the subdominant neutral exchange. We assume that the angular distribution of the right-handed slepton pair in the center of mass is the same of that of the primary decay particles, the $\tilde{\ell}_L$ and $\tilde{q}$. This is a good approximation for energies well above threshold, where most events come from, as can be seen in Fig. 6. In this limit, it is possible to define a "thrust axis," around which the decay products of the two primary final states are boosted. We then boost this distribution to the laboratory frame. The approximation made fails for energies just above threshold, for which decay products can have a more spherical distribution resulting, in principle, in larger angles and ultimately in larger track separations. However, the events among these that do make it to the detector tend to come from smaller distances than the range, therefore compensating—at least in part—the potentially larger angles. In any case, this approximation tends to underestimate the stau track separation. In the calculation we also include the additional zenith angular dependence induced by the Earth profile.

Taking the above features into consideration, we performed a simulation where we generated approximately 30k events (the numbers for each squark mass varied accordingly to the production energy threshold). These events where distributed in energy steps ranging from the stau production threshold to 10^{11} eV. For each energy we generated events for which the center of mass (CM) angular distribution was chosen based on the differential cross section distribution, as mentioned above. The 4-momentum of these events was then defined in the CM and boosted to the lab frame. With this procedure we determined the lab angular ($\Theta_{\rm lab}$) distribution. Then the neutrino-Earth interaction point (R) was chosen based on the interaction probability distribution. The separation at the detector is then simply $\Theta_{\rm lab} \times$ R.

The NLSPs track separation distribution for various squark masses is shown in Fig. 7. The rather broad distribution is characterized by track separations of hundreds of meters. For 300 GeV squark mass, 87% of the distribution is above 30 m separation, and 52% is above 100 m separation.

Another feature of the NLSP signal is that the two tracks should have very small relative angles. The angular separation of the tracks in the signal is always well below a

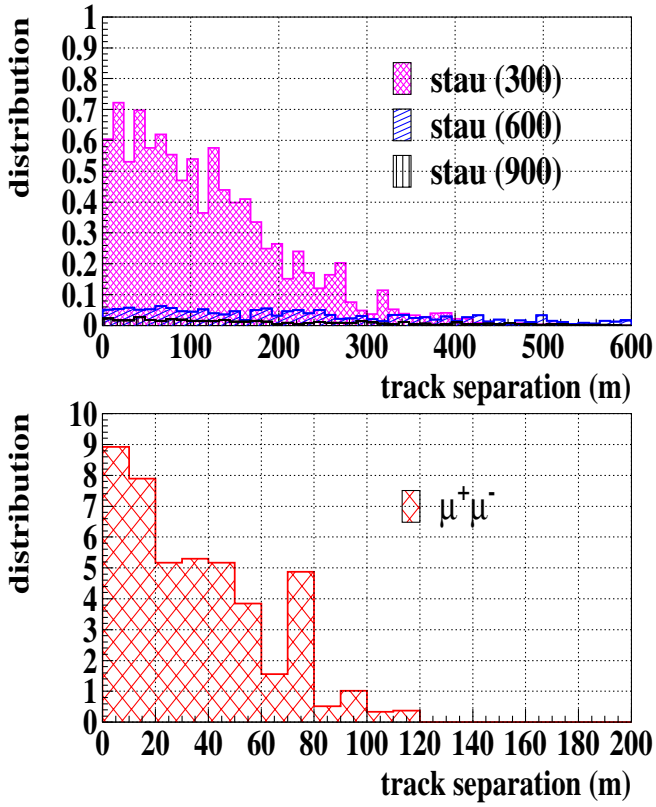

FIG. 7 (color online). Top panel: Track separation distribution of $\tilde{\ell}_R$ pair events. Bottom panel: The track separation distribution of the di-muon background. The relative normalization corresponds to the relative number of events for signal and background. Note the different horizontal scales, as well as different binning between the two figures.

degree, the typical angular resolution of neutrino telescopes, so that the tracks will appear parallel to each other. Then, most NLSP events would consist of *two* parallel but well separated tracks, and are therefore expected to be very distinctive and different from backgrounds, as we show in Sec. IV C. Given that the track separation ranges up to (300–400) m, and that the typical dimension of the detector is 1 Km, we expect that many events will be contained and therefore distinguishable from single-muon tracks. On the other hand, the typical separation appears to be large enough to distinguish the presence of two tracks in a given signal event.

The energy with which the slepton pairs arrive at the detector has a distribution which peaks just above 100 TeV, as can be seen in Fig. 8. On the other hand, the energy deposited in the detector by a typical stau track ($\simeq 800$ m which is IceCube geometrical efficiency for long tracks [10]) is approximately 160 GeV, which is small compared to its total energy. Low energy muons may mimic this energy deposition pattern, but they tend to have shorter paths in the detector. This fact can be used in order to reduce the background, as we discuss below.

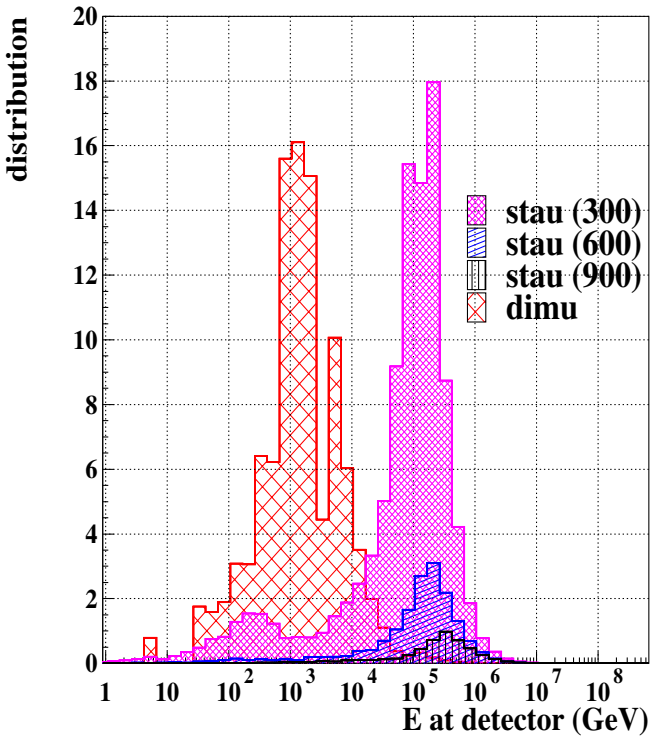

FIG. 8 (color online). Arrival energy distribution of the $\tilde{\ell}_R$ at the detector and for $m_{\tilde{q}} = 300$, 600, and 900 GeV. Here, $m_{\tilde{\ell}_R} = 150$ GeV and $m_{\tilde{w}} = 250$ GeV. Also shown is the arrival distribution for the di-muon background. The energy *deposited* in the detector by a stau traveling the average track length of 800 m is $E^{\rm dep}_{\tilde{\ell}_R} = 160$ GeV, approximately the same for all the masses considered here (see Fig. 9).

C. Backgrounds

The main potential background for the detection of NLSPs, muons produced by upgoing atmospheric neutrinos, is eliminated by asking for two tracks in the events. With the additional requirement that the tracks be almost parallel and considering the excellent time resolution of the IceCube detector, the coincidence background (two coincident muons tracks) becomes negligible.

However, there remains an important background, namely, direct di-muon production. The main source of direct di-muons is the production of charm, which subsequently decays semileptonically to a muon. That is, we consider the process

$$\nu N \to \mu^- H_c \to \mu^- \mu^+ H_x \nu,$$

where the charm hadron H_c decays according to $H_c \to H_x \mu^+ \nu$, and H_x can be a strange or nonstrange hadron. The cross section for producing a charm quark from a light d or s quark is

$$\frac{d^2\sigma(\nu N \to cX)}{d\xi dy} = \frac{G_F^2 2ME_\nu}{\pi} R^2(Q^2)\xi\left(1 - \frac{m_c^2}{2ME_\nu\xi}\right) \times \{|V_{cs}|^2 s(\xi) + |V_{cd}|^2 d(\xi)\}, \quad (4.2)$$

where $s(\xi)$ and $d(\xi)$ are the strange and down quark parton distribution functions, respectively. In Eq. (4.2) the slow scaling variable is defined as

$$\xi = x\left(1 + \frac{m_c^2}{Q^2}\right), \quad (4.3)$$

and we also defined

$$R(Q^2) = \frac{M_W^2}{M_W^2 + Q^2}. \quad (4.4)$$

The di-muon background results in a number of events larger than the signal, even for the case of a 300 GeV squark mass, as can be seen in Table I. Also, the angular separation between the di-muon tracks is, as in the case of the NLSP signal, very small and well below the projected angular resolution of neutrino telescopes. Thus, di-muon tracks will also appear to be parallel.

However, muons need to be close to the detector in order to range into it. Thus, the di-muon events have a considerably smaller separation between the two tracks than the NLSP events, which can range in from hundreds or even thousands of kilometers. This is shown in Fig. 7, where it is clear that for track separations above 100 m there should not be any significant contribution from the di-muon background. We can estimate the statistical significance of the signal as $S/\sqrt{B}$, with S and B the number of signal and background events, respectively. We could then ask what is the cut in track separation that would yield a significance equal to 5. We find that cutting events with less than 106 m separation results in 3 detectable NLSPs and 0.25 di-muons, yielding a 5σ significance.

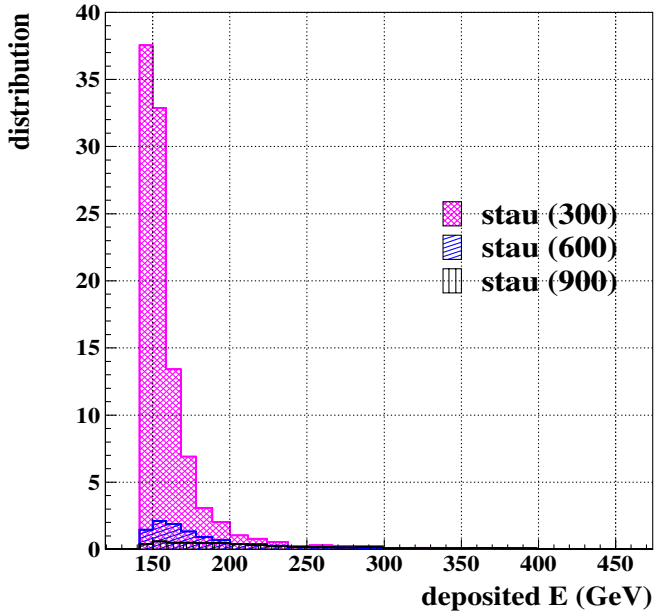

FIG. 9 (color online). Energy deposited in the detector by a right-handed stau traveling the average track length of 800 m.

It is possible to further reduce the di-muon background by making use of the energy deposition of the events. This is due to the fact that NLSPs go through the detector losing very little energy, while muons tend to deposit larger amounts of energy in the detector in such long paths. This can be seen by comparing the energy loss for a muon in Fig. 3 with that of a slepton in Fig. 5, where the largest source of energy loss for the NLSP is still 3 orders of magnitude smaller than that for the muon at the energies with which they arrive at the detector. For example, a muon with an arrival energy of 3×10^3 GeV, transversing 800 m of ice (the average through-detector length) will deposit $\sim$450 GeV in its path. This is to be compared with the deposited energy for a slepton in Fig. 9. Thus, excluding events with *deposited* energies above a few hundred GeV, we can eliminate the high energy tail of the di-muon background of Fig. 8. This can be used, in addition to the track separation cut, to further reduce the background events. The precise extent to which this method can be used to reduce the background requires further study.

Finally, there is an additional potential source of di-muons from $\nu\gamma \to W^+\mu$ scattering [20], where the γ is emitted off the parton in the nucleon and the produced $W^\pm$ decays to $\mu\nu_\mu$. However, not only is this a smaller source of di-muons, but also its track separation distribution is very similar to that of the di-muons coming from charm production and is equally eliminated by the same cut in track separation.

V. CONCLUSIONS

We have confirmed that the proposal of Ref. [3] is viable, i.e. neutrino telescopes are potentially sensitive to the relatively long-lived charged NLSPs which are present in a wide variety of models of supersymmetry breaking. Compared to Ref. [3], we have now made a detailed study of the NLSP energy loss (Sec. III). This has confirmed our estimates in Ref. [3] and is in agreement with the calculations of Ref. [6].

Regarding the analysis of the signal, we have shown that the separation between tracks will be such that we can expect that most events will be contained in a km^3 such as IceCube, whereas they will be separated enough to be identified as two distinct tracks. Moreover, we have shown that the separation between tracks is a variable that will allow one to identify the signal above the most important background, the direct production of $\mu^+\mu^-$ pairs. This is shown in Fig. 7. For instance, we have seen that a 5σ significance can be achieved with a cut of 106 m in the track separation.

Also, given that the NLSP deposits energy in the detector like a rather low energy muon, but it goes right through it like a high energy muon could, it is possible to further reduce the number of background events by making a cut in the amount of deposited energy of the events going through the detector. The details of this method of reducing the background deserves further study.

The region of the supersymmetry breaking parameter space that is available to neutrino telescopes is determined by the requirement that the NLSP lifetime be long enough to give a signal ($\sqrt{F} \gtrsim 5 \times 10^6$ GeV). Thus the observation of NLSP events at neutrino telescopes will constitute a direct probe of the scale of supersymmetry breaking. This is to be compared with the potential observation of these NLSPs at the Large Hadron Collider (LHC), where for this range of $\sqrt{F}$ the NLSP decays outside the detector and is seen through its ionization tracks. However, the observation at the LHC would not constrain the NLSP lifetime significantly. Thus, we see that neutrino telescopes are complementary to collider searches. For instance, the observation of NLSP events at the LHC, coupled to significantly fewer than expected events in neutrino telescopes, would point to $\sqrt{F} < 10^7$ GeV.

The event rates shown in Table I are already encouraging for experimental facilities that are being built, such as IceCube. Future upgrades of IceCube [21] will result in even better sensitivity. The water detectors ANTARES [22], NESTOR [23], and NEMO [24] will also be able to look for these NLSPs.

Finally, in the present work we focused on supersymmetry. However, other theories give rise to relatively long-lived charged particles which can be observed by neutrino telescopes [25]. A large portion of this work could be applied to these other scenarios with little modification.

ACKNOWLEDGMENTS

We thank M. Alhers, J. Kersten, and A. Ringwald for helpful comments that led us to find an error in an earlier

version of this paper. I. A. and G. B. acknowledge the support of the State of São Paulo Research Foundation (FAPESP). G. B. also thanks the Brazilian National Counsel for Technological and Scientific Development (CNPq). Z. C. is supported by the NSF under Grant No. PHY-0408954.

[1] M. Dine, W. Fischler, and M. Srednicki, Nucl. Phys. **B189**, 575 (1981); S. Dimopoulos and S. Raby, Nucl. Phys. **B192**, 353 (1981); L. Alvarez-Gaumé, M. Claudson, and M. B. Wise, Nucl. Phys. **B207**, 96 (1982); M. Dine and A. E. Nelson, Phys. Rev. D **48**, 1277 (1993); M. Dine, A. E. Nelson, and Y. Shirman, Phys. Rev. D **51**, 1362 (1995); M. Dine, A. E. Nelson, Y. Nir, and Y. Shirman, Phys. Rev. D **53**, 2658 (1996). For a review, see G. F. Giudice and R. Rattazzi, Phys. Rep. **322**, 419 (1999).

[2] J. L. Feng, A. Rajaraman, and F. Takayama, Phys. Rev. Lett. **91**, 011302 (2003); Phys. Rev. D **68**, 063504 (2003); J. L. Feng, S. f. Su, and F. Takayama, Phys. Rev. D **70**, 063514 (2004); J. L. Feng, S. Su, and F. Takayama, Phys. Rev. D **70**, 075019 (2004).

[3] I. Albuquerque, G. Burdman, and Z. Chacko, Phys. Rev. Lett. **92**, 221802 (2004).

[4] J. Ahrens *et al.* (The IceCube Collaboration), Nucl. Phys. B, Proc. Suppl. **118**, 371 (2003).

[5] X. J. Bi, J. X. Wang, C. Zhang, and X. m. Zhang, Phys. Rev. D **70**, 123512 (2004).

[6] M. H. Reno, I. Sarcevic, and S. Su, Astropart. Phys. **24**, 107 (2005).

[7] M. Ahlers, J. Kersten, and A. Ringwald, J. Cosmol. Astropart. Phys. 07 (2006) 005.

[8] S. I. Dutta, M. H. Reno, I. Sarcevic, and D. Seckel, Phys. Rev. D **63**, 094020 (2001).

[9] E. V. Bugaev and Y. V. Shlepin, Phys. Rev. D **67**, 034027 (2003).

[10] For a detailed discussion of neutrino event rates, see I. Albuquerque, J. Lamoureux, and G. F. Smoot, Astrophys. J. Suppl. Ser. **141**, 195 (2002).

[11] S. Eidelman *et al.* (Particle Data Group), Phys. Lett. B **592**, 1 (2004).

[12] D. E. Groom, N. V. Mokhov, and S. I. Striganov, At. Data Nucl. Data Tables **78**, 183 (2001).

[13] S. R. Kelner and Y. D. Kotov, Yad. Fiz. **7**, 360 (1968) [Sov. J. Nucl. Phys. **7**, 360 (1968)].

[14] R. P. Kokoulin and A. A. Petrukhin, Acta Phys. Acad. Sci. Hung., Suppl. **29**, 277 (1970).

[15] H. Abramowicz, E. M. Levin, A. Levy, and U. Maor, Phys. Lett. B **269**, 465 (1991).

[16] H. Abramowicz and A. Levy, hep-ph/9712415.

[17] E. Waxman and J. N. Bahcall, Phys. Rev. D **59**, 023002 (1998); J. N. Bahcall and E. Waxman, Phys. Rev. D **64**, 023002 (2001).

[18] K. Mannheim, R. J. Protheroe, and J. P. Rachen, Phys. Rev. D **63**, 023003 (2000).

[19] R. Gandhi, C. Quigg, M. H. Reno, and I. Sarcevic, Astropart. Phys. **5**, 81 (1996); Phys. Rev. D **58**, 093009 (1998).

[20] D. Seckel, Phys. Rev. Lett. **80**, 900 (1998).

[21] F. Halzen and D. Hooper, J. Cosmol. Astropart. Phys. 01 (2004) 002.

[22] J. A. Aguilar *et al.* (The ANTARES Collaboration), Yad. Fiz. **67**, 1195 (2004) [Phys. At. Nucl. **67**, 1172 (2004)].

[23] P. K. F. Grieder (NESTOR Collaboration), Nuovo Cimento C **24**, 771 (2001).

[24] NEMO Collaboration, http://nemoweb.lns.infn.it/.

[25] I. Albuquerque, G. Burdman, C. Krenke, and B. Nosratpour (unpublished).